A modern analog analysis of the relationship between Northern and Southern East Asian summer monsoon regions, with an application to the paleoclimate of the past 1000 years

by

Fei Ma

A thesis submitted in partial fulfillment of the requirements

for the degree of Master of Science

Department of Geography

University of Wisconsin Madison

Nov. 27, 2011

Acknowledgements

First and foremost, I would like to express my sincere gratitude to my advisor Prof. Joe Mason, for his inspiration on research ideas, patience and explicit in explaining concepts, immense knowledge and tremendous support through the whole process of my Master's study. My sincere thanks also go to the other two professors on my committee, Prof. Jim Burt and Prof. Jack Williams for their valuable suggestions. I have to mention also the talks with Dr. Guangshan Chen from UW-Madison and Prof. Michael Gill from UCLA, that inspired me on proposing this larger-scale mechanism in the thesis to explain the dipole system. Thank Karen Russ and Jiaxu Zhang too, for the valuable suggestions and patient explanations they provided. I would also like to thank the colleagues, secretaries and librarians from Geography department who created the great study and research environment. Last, I'm deeply grateful to my parents and my friends, who gave me a lot of support and help in many different ways.

Abstract

Recent studies have identified a precipitation dipole (i.e. two regions in which precipitation changes are consistently out of phase with each other) between the Northern and Southern East Asian Summer Monsoon regions (NEASM/SEASM) during the past 1000 years. To explore the mechanism for this pattern, NCEP reanalysis data of the past 63 years (1948-2010) are used in a modern analog analysis. The precipitation rate shows a distinct shift around the year 1978, from high to low for NEASM, and in the opposite direction for SEASM. Differences in zonal flow (uwind/vwind), geopotential heights, vertical motion (omega) and sea-surface temperature (SST) in the western Pacific before and after 1978 were analyzed to identify underlying mechanisms. Based on this analysis, local changes in vertical motion in the two regions contributed to the out-of-phase pattern. Also significant to the rainfall anomalies is the SST of the Philippine Sea. A shift to lower SST in this region around 1978, similar to the SST anomaly observed there during El Niño events, served as the triggering factor for larger-scale changes in circulation patterns. First, a convection anomaly in the Northwest Pacific (NWP) affects the ascent in the Indian Summer Monsoon region (ISM), which has a teleconnection with the Mediterranean/Aral Sea regions via Rossby waves. Then, the Asian Jet transmits a potential vorticity anomaly from that region eastward to the NEASM. The SEASM, on the other hand, is affected mostly by the anomalous meridional wind originating

from the SST anomaly in the Philippine Sea. The combination of local subsidence and large-circulation patterns explains the dipole pattern of NEASM and SEASM in recent decades. A decadal to multi-decadal scale dipole in aridity is also evident in high-resolution paleoclimatic reconstructions for the Medieval Warm Period in East Asia, and can also be explained with a similar mechanism.

Table of Contents

Introduction

1 East Asian Summer Monsoon (EASM)

The EASM brings roughly 70% of the total annual precipitation to East Asia, and is of great significance for agricultural activities (Shen et al., 2008). The livelihood and well-being of monsoon societies (India, Japan, etc.) depend to a large extent on the EASM. With high variability of rainfall the monsoon region may suffer from droughts or floods (Wang, 2006). Today in the context of global warming, related changes in the behavior of East Asian Monsoon (both summer and winter) are a major concern to the populace of this region.

The summer monsoon normally begins in early to mid-May. The difference in heat capacity between land and sea creates a temperature contrast, with the Tibetan plateau acting as an elevated heat source. The pressure gradient resulting from this temperature contrast results in the monsoon winds, which carry moisture into the EASM region. Heavy convective rainfall develops over southern China along the pre-Meiyu front. It is then followed by northward shifts of the summer monsoon, causing an elongated rain belt referred to as Meiyu or 'Plum Rains' (Baiu in Japanese) rainy season lasting through June and July over the Yangtze River Valley in southeastern China. The Meiyu-Baiu front then shifts northward in July and brings abundant rainfall to northeast China and Japan. At the end of August, the summer monsoon begins to withdraw southward.

The large-scale onset of the Asian monsoon rainy season consists of two phases. The first phase is the rainfall surge over the South China Sea (SCS) during mid-May. This establishes a planetary-scale monsoon rain-band extending from the marginal seas (the Arabian Sea, the Bay of Bengal, and the SCS) to the subtropical western North Pacific (WNP). In June, the rain-band advances northwestward to India, southeast China (where it is called the Mei-yu), Korea (Jangma) and Japan (Baiu). In late July and early August it approaches northern China. The rainy season then retreats southward over East Asia in late August. (Wang and Lin, 2002)

2 EAM dipole in the past millennium

The 'Medieval Warm Period' (MWP) (AD 1000–1300) and the 'Little Ice Age' (LIA) (ad 1500–1850) (Lamb, 1977) were characterized by unusually high and low temperatures respectively in many parts of the world, as well as moisture anomalies in some regions. It has proven to be difficult to reconstruct large-scale changes in precipitation, as opposed to temperature, during these time periods due to the heterogeneous nature of hydroclimatic variables. More information on hydroclimatic variation during these recent parts of the Holocene is important, in part because researchers have noticed possible relationships between human society and precipitation anomalies. For example, population density and intensity of agricultural activities were generally larger than any previous time in the NEASM area during Liao and Jin Dynasties (AD 916 to AD 1234) when it is believed that the climate was relatively wet (Ren, 1998). The development, decline and disappearance of Harappan

civilization in India between 9000 and 3000 cal BP occurred at about the same time as a decreasing western equatorial Pacific SST and increasing frequency and amplitude of ENSO events, associated with increasing aridity in northwestern India (MacDonald, 2011). The Mayan civilization also declined when their region suffered from continuous severe droughts (Hodell et al., 2001).

The MWP has been discussed as a possible analog for changes in circulation and hydroclimate associated with current and future global warming. Although the climate similarities between the MWP and present trends depend on the specific region, three relatively warm intervals (1010–1040, 1070–1105, and 1155–1190) have been identified as comparable to the mid-20th century warm period (Crowley and Lowery, 2000). A modern analog approach to interpreting the MWP climate in East Asia using observations from recent decades could therefore be valuable both for understanding synoptic patterns of climate during the MWP and for predicting future change in the same region.

Previous research has identified the driving factors of variations in the monsoon system at various timescales, and this work can be used to interpret changes inferred from paleoclimatic records as well as those that occurred in recent decades. Over glacial-interglacial time scales, precession-driven variations in seasonal insolation are the main pacemaker of the Asian monsoon (e.g. Clemens et al., 2003). It has also been proposed that a 1500-yr cycle in Holocene monsoon dynamics is driven by variation in solar activity (e.g. Gupta et al., 2005). Centennial-scale oscillation may be linked to Gleissberg cycles, a form of solar forcing, as suggested by Zhu and Wang (2002).

A quasi 50–60-yr interdecadal fluctuation is observed in the South Asian summer monsoon, the East Asian summer monsoon, and ENSO (Goswami, 2006). Goswami hypothesized that this oscillation of the Asian monsoons and ENSO is a manifestation of a global coupled ocean-atmosphere mode of oscillation. Based on PCA analysis of observational, proxy (historical data), and modeled results, Shen et al. (2008) pointed out that a pentadecadal oscillation is strong during both warm and cold episodes in the last millennium, with NEASM and SEASM out-of-phase with each other during the MWP. They proposed that this has to do with the fluctuation of ENSO and PDO (Pacific Decadal Oscillation), but did not expand on the mechanisms for the fluctuation of at this timescale. Interdecadal and multidecadal variations of the South Asian summer monsoon have been investigated in detail for the past millennium (Wang, 2006). Less has been done, however, on exploring the underlying mechanisms of the precipitation anomalies over that time period, especially the contrasts noted between NEASM and SEASM regions. At the shortest timescales, seasonal to interannual, ENSO and the Quasi-biennial Oscillation (QBO) are seen as the primary controls of precipitation over East Asia (Waliser, 2006; Yang and Luo, 2006). Thus, ENSO may play a role in monsoon variations over multiple timescales.

3 Teleconnections and dipoles

Rodwell and Hoskins (1996) suggest that diabatic heating in the Asian monsoon region can induce a Rossby-wave pattern in remote regions to the west. The warm thermal structure interacts with air on the southern flank of the mid-latitude westerlies,

which causes it to descend over the Mediterranean. Other researchers have suggested more far-reaching teleconnections between the Asian monsoons and climate in other regions. For example, it has been proposed that when the East Asian Monsoon gets stronger, a decrease in precipitation would occur in North Africa (Lau, 1992; Liu et al., 2008).

Zahn (2003) suggests that the monsoon subsystems (the Asian, Indian and African monsoons) are all connected with the variation of sea surface temperatures in the oceans. In modern observations, both South and East Asian monsoons are found to be both closely related with sea surface temperature anomalies (SSTA) of the northwest Pacific (NWP) and ENSO (Wang, 2006). For example the strength of the Indian Summer Monsoon (ISM) is negatively correlated with sea surface temperatures (SST) in the eastern and central equatorial Pacific Ocean, and is positively correlated with temperatures in the western equatorial Pacific (MacDonald, 2011).

The EASM is also connected with SST anomalies in the Pacific (Wang, 2006). Rainfall tends to be significantly greater in the summer after an El Niño event. For example, the devastating Yangtze River floods in the summer of 1998 that followed the 1997 El Niño (Lau and Weng 2001). Data from the last half-century reveals a shift in the precipitation in EASM region as well as the SST in the NWP around the mid-1970s (Wang, 2006).

The relationship between these subsystems is shown in Fig 1, from Zahn (2003). For the Northern Hemisphere especially, the Circum-global Teleconnection (CGT) is associated with the westerly jet stream (Ding and Wang, 2005), and correlates with ISM

and ENSO. ENSO and EAM are closely related with each other. It has been suggested that the multidecadal variation of summer precipitation over eastern China is associated with the internal process of the ocean-atmosphere, such as ENSO events and PDO (Li et al., 2005; Zhou et al., 2006). The SST of Niño 3 region (150°W-90°W, 5°S-5°N) experienced also the shift from week to strong in late 1970s (Nitta and Yamata 1989; Trenberth and Hurrell 1994).

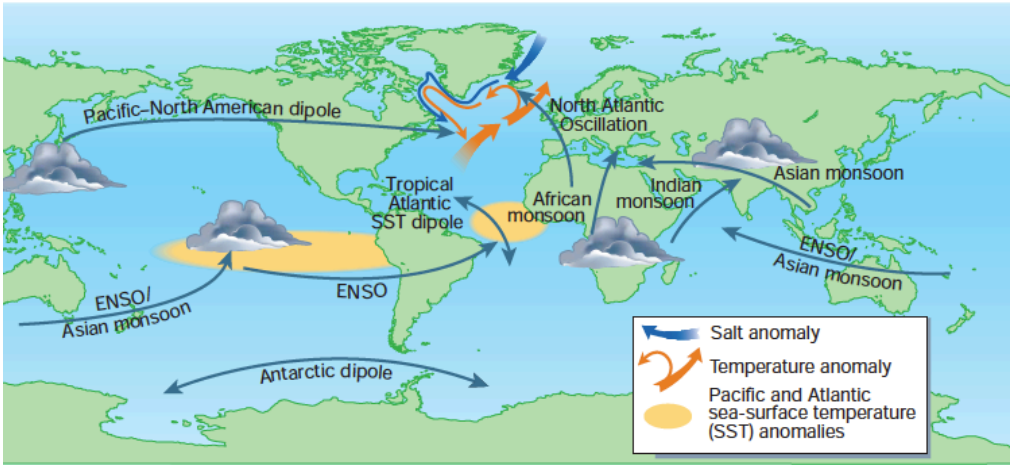

Fig. 1. Monsoon-SST teleconnection (Zahn, 2003)

With that background, it is clear that teleconnections involving large-scale circulation may be significant for changes in precipitation within the EASM region(Wang, 2006). However, it is also important to consider the details of local shifts in atmospheric circulation such as local uplift/subsidence patterns . These more local systems are less investigated than global teleconnections but they are important for at least two reasons. First, as the local response to large-scale circulation changes, they

may represent an important part of the overall teleconnection mechanism. Second, they may be influenced by change in local factors, for example, a change in land cover that alters the surface energy balance.

Recent studies have identified an apparent dipole between the core of monsoon system and its edges (usually in the form of deserts) in the dune fields of Inner Mongolia, China during the early to mid-Holocene (Mason et al., 2009), and an uplift/subsidence system is proposed as the explanation. The enhanced precipitation in the monsoon center is considered to be associated with relatively drier conditions in surrounding areas, probably due to atmospheric subsidence, analogous with a similar dipole noted for the southwestern monsoon in the U.S. (Higgins et al., 1997, 1998; Higgins and Shi, 2000; Harrison et al., 2003). The rising motion of air mass results in uplift, adiabatic cooling and condensation of moisture, therefore it is also critical for precipitation.

4 Modern analog analysis and its application in this thesis

Modern analog analysis is a method used by paleoclimatologists to explain patterns revealed by paleoclimatic proxies by matching them to similar patterns in modern atmospheric data. Specifically, past circulation patterns simulated by GCMs are matched with those recorded by modern instruments, which come with finer resolution as well as more details (Mock and Bartlein, 1995). Modern analog analysis is based on the assumption that present broad-scale atmospheric circulation patterns, surface-climate responses, and the mechanisms linking them are similar to those believed to have

occurred in the past. Modern analog analysis doesn't reconstruct paleoclimate; instead it provides valuable information on atmospheric processes that may have led to certain past climatic patterns, and can help to determine what influences local or large-scale controls may have on precipitation patterns of the past (Shinker et al., 2006). Modern analogs can also be used to test the plausibility of paleoclimatic hypotheses suggested by GCM simulations or paleoclimatic data (Edwards et al., 2001). With this method, Shinker et al. (2006) investigated the synoptic and dynamic climate controls of North American aridity in the early Holocene. Mock and Brunelle-Daines (1999) also applied this concept to the summer paleoclimate of 6 ka BP in the western United States. The modern analog approach has even proved to be applicable to climatic changes of the Late Pleistocene at regional scales where synoptic features are most important (Mock and Bartlein, 1995).

In this thesis, a modern analog approach is used to identify possible mechanisms that would produce a precipitation dipole between northern and southern parts of the East Asian Monsoon region, including the broader teleconnections discussed above. The NCEP reanalysis of modern observations is first used to compare the timing and direction of recent decadal-scale precipitation shifts in the NEASM and SEASM. Other NCEP variables are then used to assess broader changes in circulation and SST associated with precipitation shifts, and a conceptual model is proposed to explain out-of-phase precipitation changes in the NEASM and SEASM. Finally, high-resolution paleoclimatic reconstructions from the past 1000 years are used to evaluate whether

this conceptual model can also be applied to the East Asian Monsoon during the Medieval Warm Period.

Data and Methods

Analysis of precipitation requires comprehensive information regarding atmospheric circulation and vertical motions (Webster et al., 1998). Monthly mean and long-term mean data in netCDF(.nc) files from the year 1948 to 2010 were downloaded from the NCEP/NCAR 50-year Reanalysis Project (http://www.esrl.noaa.gov/psd/data/reanalysis/reanalysis.shtml).

Based on previous evidence for out-of-phase precipitation changes in the northern and southern parts of the East Asian monsoon regions (Tan et al., 2007; Shen et al., 2008), two distinct regions were selected for analysis: the North East Asian Summer Monsoon (NEASM) and South East Asian Summer Monsoon (SEASM) areas (Fig. 2).

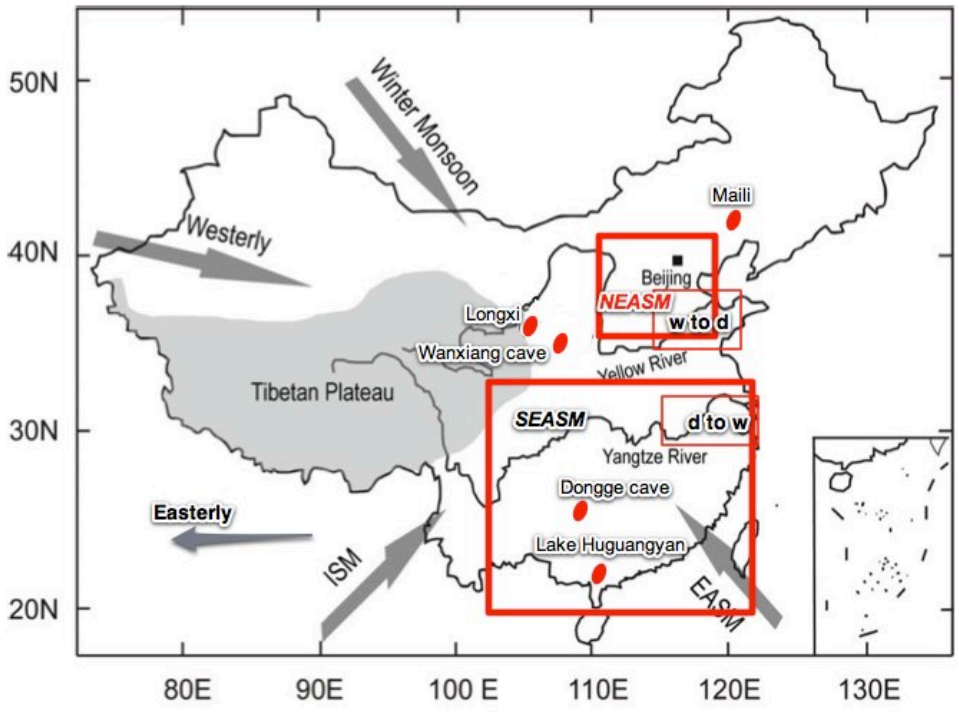

Fig. 2 Two anomalous precipitation rate regions (NEASM and SEASM). Two small boxes indicate the change in moisture conditions from MWP to LIA (Shen et al., 2008). Locations of proxy data used in this paper are also denoted: Wanxiang Cave (Zhang et al. 2008), Dongge Cave (Wang et al., 2005), and Lake Huguangyan (Chu et al., 2002) (Adapted from Tan et al., 2007)

The NCEP variable used was *prate*, monthly mean precipitation rate ($kg/m^2/s$). A 63-year time series of summer (June, July, August) precipitation rate anomalies from 1948 to 2010 was calculated for each region as follows: The long-term mean summer precipitation (1948-2010) was subtracted from the summer precipitation rate for each year, after averaging yearly and long-term mean rates over the NEASM and SEASM regions respectively (Fig. 3). The resolution is 1.875°×1.904°. The resulting precipitation series was then used to identify major decadal-scale change in precipitation between the two regions, for analysis of possible out of phase behavior and mechanisms that could explain it. For this purpose, the regime shift method (Rodionov, 2006), provides a way to detect shifts in the mean level of climate variables, was used. If the hypothesis that mean values of two time periods are equal is rejected by the two-tailed Student t-test, then a shift is determined. A QQ Plot of the precipitation rate reveals that the data satisfy the normal assumption for t-test. This method provides an alternative to the running average method in detecting shifts in the mean (Yang and Lau, 2004). The three parameters chosen to implement Rodionov's method were:

1.Significance level: 0.05

2.Cut-off length (only regimes longer than this time span will be detected): 10, 20, and 40 years (to detect decadal variations)

3.Huber's weight (controls the weights assigned to the outliers): 6 sigma (If anomalies are less than or equal to 6 sigma then their weights are equal to one. Otherwise, the weights are inversely proportional to the distance from the expected mean value of the new regime.)

The regime shift analyses for the NEASM clearly show that the year 1978 stands out as a shift point, regardless of whether 10, 20 or 40 years is used as the cut-off length (Fig. 3, right side). As for the SEASM region, a shift is detected in 1985 for the 20 and 40 year cutoff lengths, while the 10 year cutoff yields a shift a few years later (left panel of Fig. 3). Shifts were also detected at 2005-2008 for the two shorter cutoff values, but there are not enough data after 2005 to allow investigation of those shifts.

The differences in weighed precipitation rate after the shift for SEASM and NEASM regions are respectively $4.4E^{-6}$ and $2.6E^{-6}$ $kg/m^2/s$, which are approximately 3.4cm and 2.0cm when averaged over the three summer months.

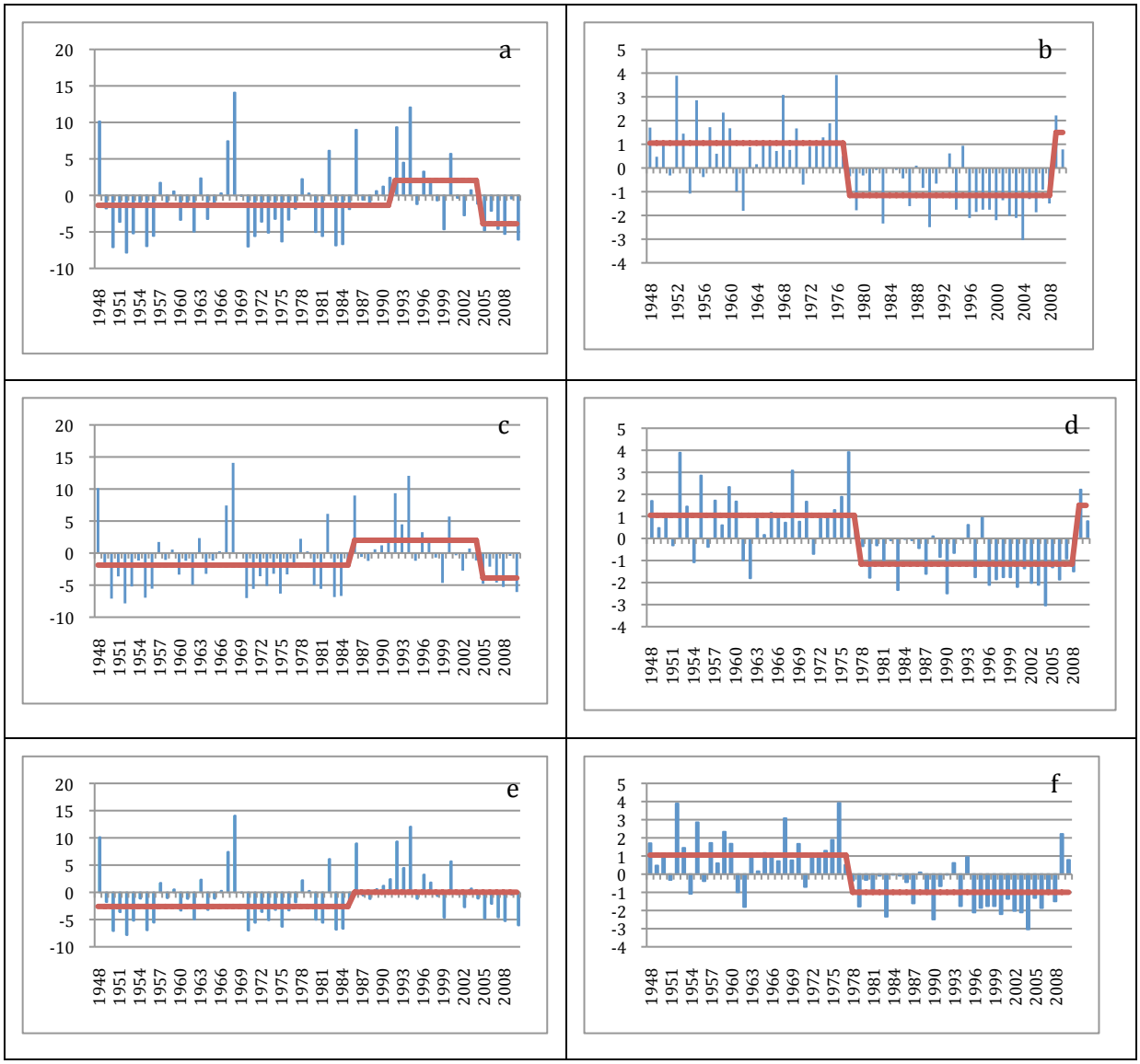

Fig. 3 Summer average precipitation for two regions (left panel: SEASM; right panel: NEASM. Cut-off length: a, b: 10 years; c, d: 20 years; e, f: 40 years. Red line: mean values for each regime. Y-axis: Precipitation (cm))

The shifts at 1978 (NEASM) and 1985 (SEASM) are in opposite directions, so for most years from 1948 to 2010, multidecadal episodes of high and low precipitation were largely out of phase between the two regions. To examine the mechanisms for

these shifts, contrasts in other variables before and after the shifts in precipitation were investigated. A breakpoint of 1978 was used, because the shift at this time in the NEASM is so well-defined regardless of cutoff length. Although the shift was several years later in the SEASM, average values of the variables of interest after or before 1978 should not be too different from the averages after or before 1985.

The following NCEP variables related to atmospheric circulation and ENSO were selected for the analysis: omega (vertical pressure velocity, Pascal/s), uwind (zonal wind, m/s), vwind (meridional wind, m/s), hgt (geopotential height, m), and Phillipine Sea SST (sea surface temperature, C°). The resolution for these parameters in NCEP is 2.5°×2.5°.

Omega at 500mb level is chosen to reflect vertical motions of the atmosphere. Values of monthly mean subtracted by long term mean indicate abnormal years of subsidence (positive) and uplift (negative). Shinker et al. (2006) pointed out that local subsidence is a more significant factor in the precipitation anomalies in North America compared with to indices of large-scale atmospheric circulation. The 200mb, 500mb, and 850mb geopotential heights, and the winds at those levels are investigated to understand the changes in large-scale circulation associated with the shift in precipitation in the NEASM and SEASM regions around 1978. We use SST of Phillipine Sea (Wang, 2006) as an index of anomalies associated with the tropical Pacific Ocean which are known to influence the EAM at the timescale of ENSO, and may also affect it at the decadal timescales that are of interest here.

Application of the modern analog analysis to climates of the past 1000 years involved two types of data. First, studies that provide proxy evidence of climate change from the past 1000 years, regardless of resolution, were reviewed for any indication of contrasting moisture conditions in the NEASM and SEASM regions. Second, high-resolution reconstructions of precipitation from speleothems of Wanxiang Cave (Zhang et al. 2008) and Dongge Cave (Wang et al., 2005) were used to investigate decadal-scale relationships between the NEASM and SEASM during the Medieval Warm Period.

Results and Discussion

1 Relationship between Precipitation Rate and Vertical Index

The SEASM region experienced higher precipitation after the year 1978, while for NEASM the change was in the opposite direction.

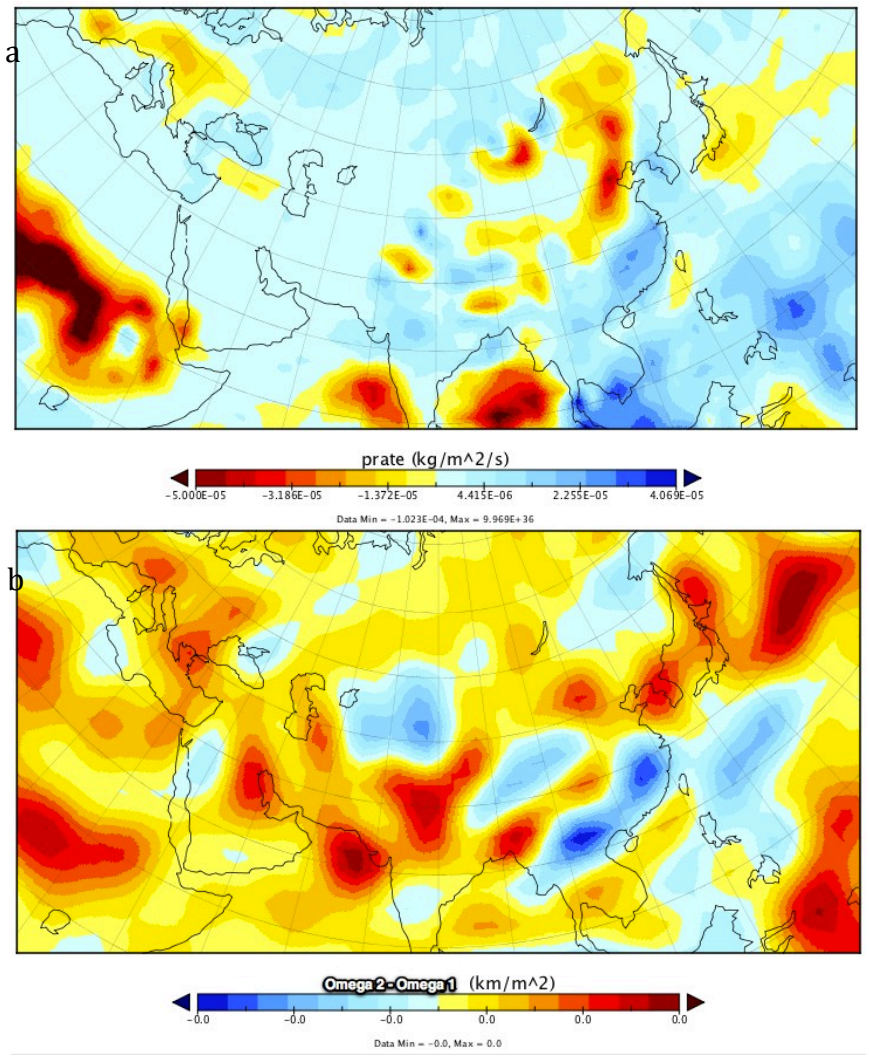

Fig. 4 Maps of the difference between pre-1978 and post-1978 means of JJA precipitation rate and vertical motion (omega) in JJA. Long term mean values of prate (a) and omega (b) before1978 were

subtracted from mean value after 1978. Negative values (blue colors) indicate a higher prate (i.e. wetter conditions) after 1978 and stronger upward motion. Positive values (red color) indicate the regions with stronger downward motion, or weaker sinking motion.

After 1978 at the 500 mb level in the atmosphere, the NEASM region experienced more subsidence, while SEASM had more uplift. On the other hand, positive values (warm color) indicate weaker convection or greater subsidence in areas such as Indonesia, the Philippine Sea, Northwest India, the Mediterranean, NEASM, and Japan. As demonstrated by Fig. 4, changes in mean omega values (north positive and south-negative) are clearly associated with the north-dry and south-wet pattern after 1978. Increased descending motion reduces the local humidity through both increased low-level divergence and greater dry vertical advection (Li et al., 2010).

The area of increased subsidence includes not only the NEASM but also Japan and Korea. The precipitation change for those regions, however, is not homogeneous. Wang (2006) and Wu and Wang (2002) point out that the barotropic anticyclone over Japan Sea during the earlier episode became a cyclone, which corresponds to the increased precipitation in this region in Fig. 4a.

2 Relationships between Precipitation Rate and Circulation Index

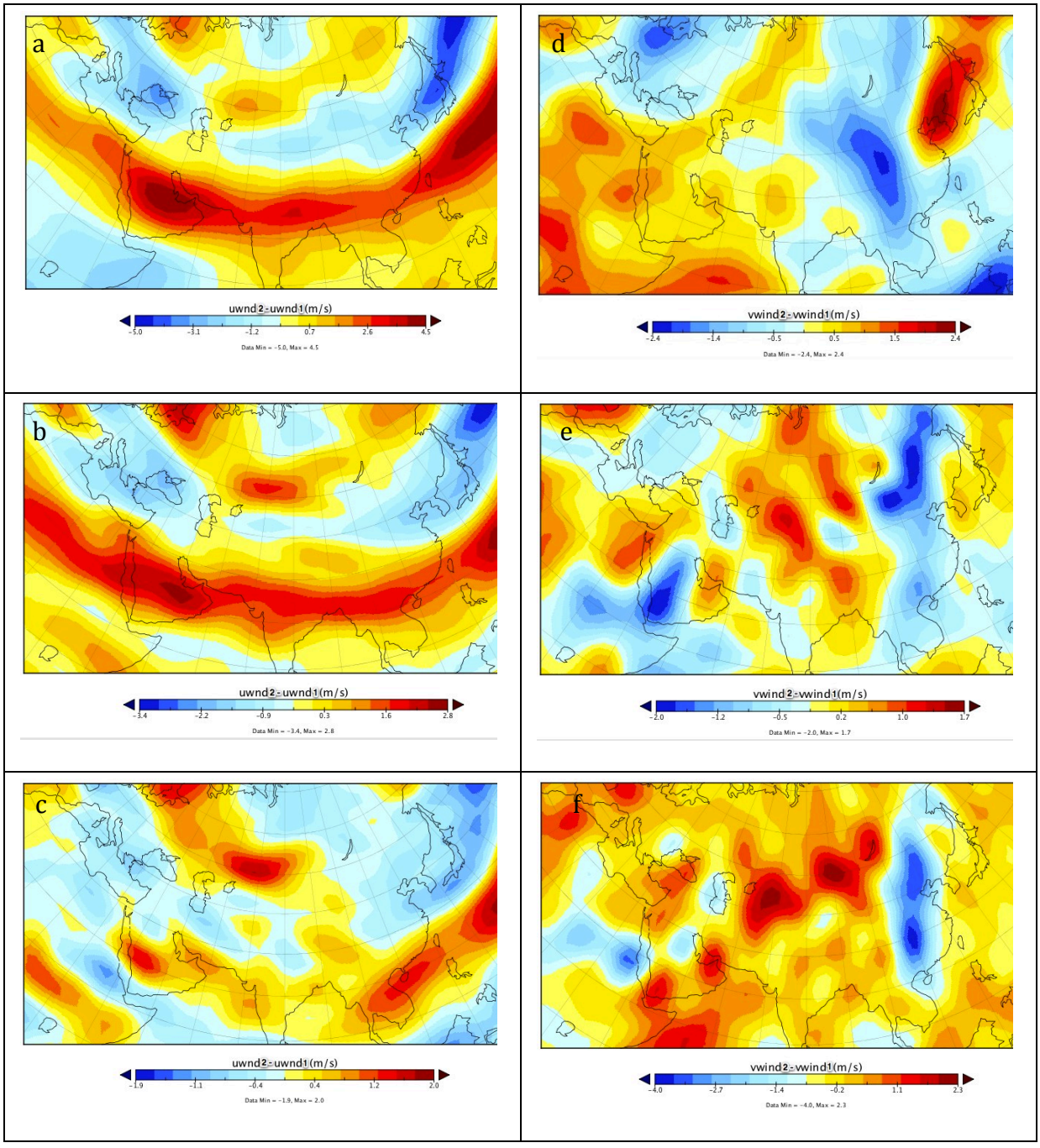
a
uwnd2-uwnd1(m/s)
-5.0 -3.1 -1.2 0.7 2.6 4.5
Data Min = -5.0, Max = 4.5
d
vwind2-vwind1(m/s)
-2.4 -1.4 -0.5 0.5 1.5 2.4
Data Min = -2.4, Max = 2.4
b
uwnd2-uwnd1(m/s)
-3.4 -2.2 -0.9 0.3 1.6 2.8
Data Min = -3.4, Max = 2.8
e
vwind2-vwind1(m/s)
-2.0 -1.2 -0.5 0.2 1.0 1.7
Data Min = -2.0, Max = 1.7
c
uwnd2-uwnd1(m/s)
-1.9 -1.1 -0.4 0.4 1.2 2.0
Data Min = -1.9, Max = 2.0
f
vwind2-vwind1(m/s)
-4.0 -2.7 -1.4 -0.2 1.1 2.3
Data Min = -4.0, Max = 2.3

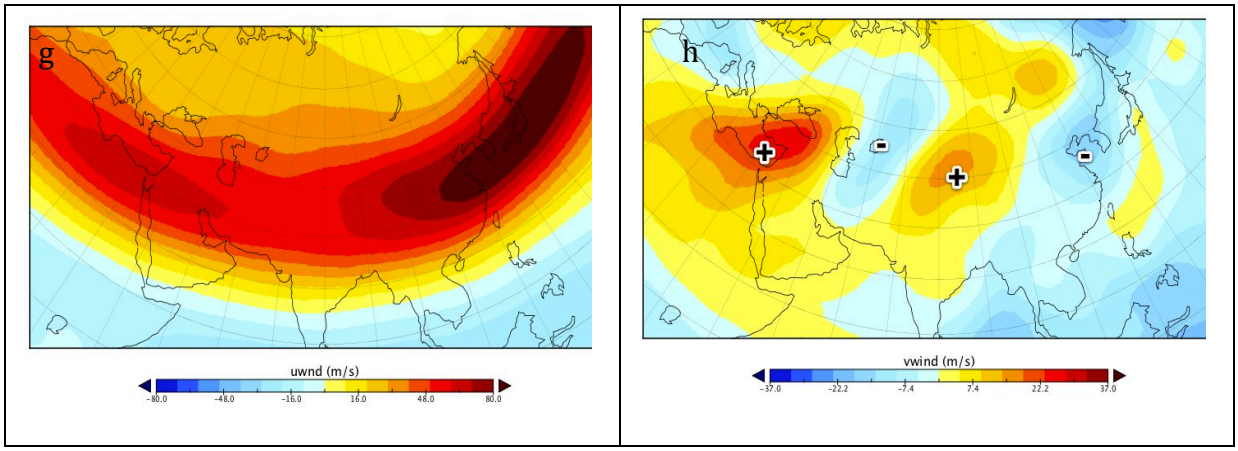

Fig. 5 Upper left panels show difference between pre- and post-1978 means of JJA uwind at 200mb level (a), 500mb level (b), and 850mb level (c). Upper right panels show pre- and post-1978 difference of JJA vwind at 200mb level (d), 500mb level (e), 850mb level (f). Lower two panels show long term mean (ltm, 1948-2010) of JJA vwind (g) and uwind(h) at the 200mb level. In Fig. 5a, b, and c, warm color indicates more intense eastward motion or weaker westward motion during summer (JJA). In Fig. 5d, e, and f, positive values (warm color) indicate strengthened northerlies, or weakened southerlies after 1978; while negative values (cold color) denotes regions with stronger southerlies or weaker northerlies

It is clear that the easterly flow stretching from East China Sea across North India to the Sahara is weaker after 1978, especially at 200 and 500 mb (Fig. 5). For the region to the north, where westerly flow prevails from the Mediterranean to central Japan (Fig. 5g), the cool color indicates weaker westerlies, again most pronounced at the two higher levels. According to Enomoto (2004), the Asian jet will be less effective in its role as wave-guide for transporting Potential Vorticity anomalies to the east.

With regard to the meridional flows, enhanced southward flow over the NEASM region after 1978 enhanced aridity there. On the other hand, the northward vwind

anomalies over the South China Sea bring more water vapor to SEASM regions, generating larger-than-normal precipitation.

Additionally, the "+-+-" pattern in Fig 5h corresponds well with the "silk road" teleconnection mentioned in the work of Enomoto (2003). PV anomalies will be transported two wavelengths from the jet entrance to the exit, enhancing development of the Bonin High over Japan and Korea. However, a "-+-+" pattern can be clearly identified in Fig. 5d, decreasing the jet stream and thus the teleconnection between Mediterranean and EASM/Bonin region after the year 1978.

3 Relationships between Precipitation Rate and Pressure Index

Greater development of middle-to-low level subtropical ridge after 1978 (warm colors) in the western Pacific over the Philippine Sea is identifiable in Figures 6b and c, echoing with the findings of Chang et al. (2000a). This anomalous Philippine Sea anti-cyclone is caused by a positive thermodynamic feedback between atmospheric Rossby waves and the underlying warm pool ocean, and is closely correlated with the oscillation of Nino 3 region (Wang et al. 2000). The strengthening of this western Pacific subtropical ridge may affect precipitation in the lower reach of the Yangtze River valley (Wang and Zhang, 2002; Chang et al., 2000a).

The region to the north of the high pressure center, including NEASM and most of Japan, experienced lower geopotential heights, especially for 200 and 500 mb, after

1978 (cool colors). This corresponds to the omega anomaly in Fig. 4b as well: more sinking/less rising in NEASM/Japan, while more rising/less sinking in SEASM.

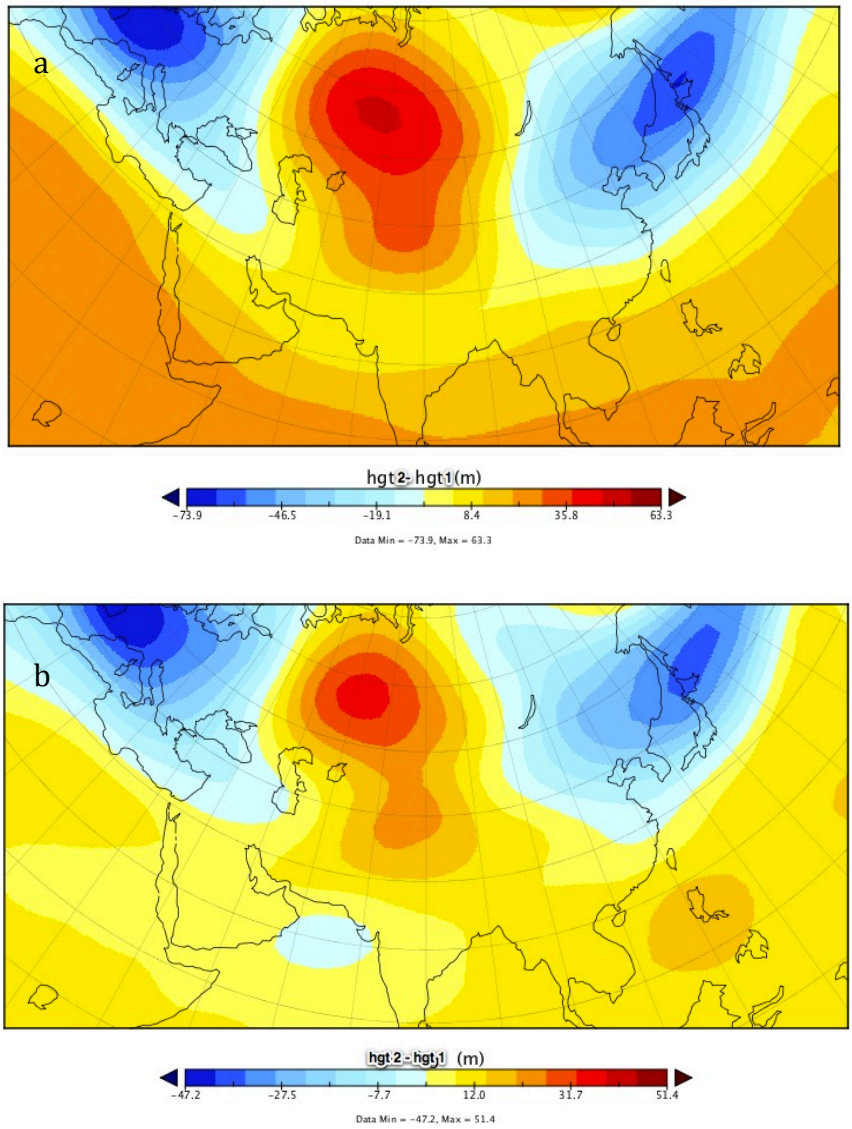

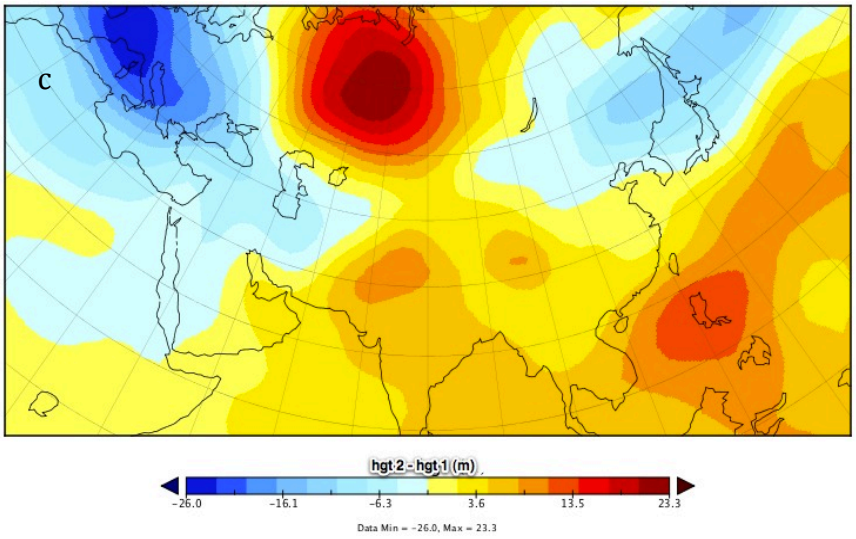

Fig. 6. Mean JJA geopotential height after1978 minus height before 1978, at a. 200mb b. 500mb c. 850mb level

4. Relationship between Precipitation Rate and SST

The pattern of change in SST before and after 1978 (Fig. 7c) is similar to a pattern observed during El Niño years, with low SST in the Philippine and surrounding areas of the western Pacific. Precipitation changes in the SEASM and NEASM regions are also associated with ENSO; therefore, it is worth reviewing the overall pattern of linked SST and circulation changes connected with ENSO to evaluate whether they are similar with the decadal precipitation changes that are the focus of this study.

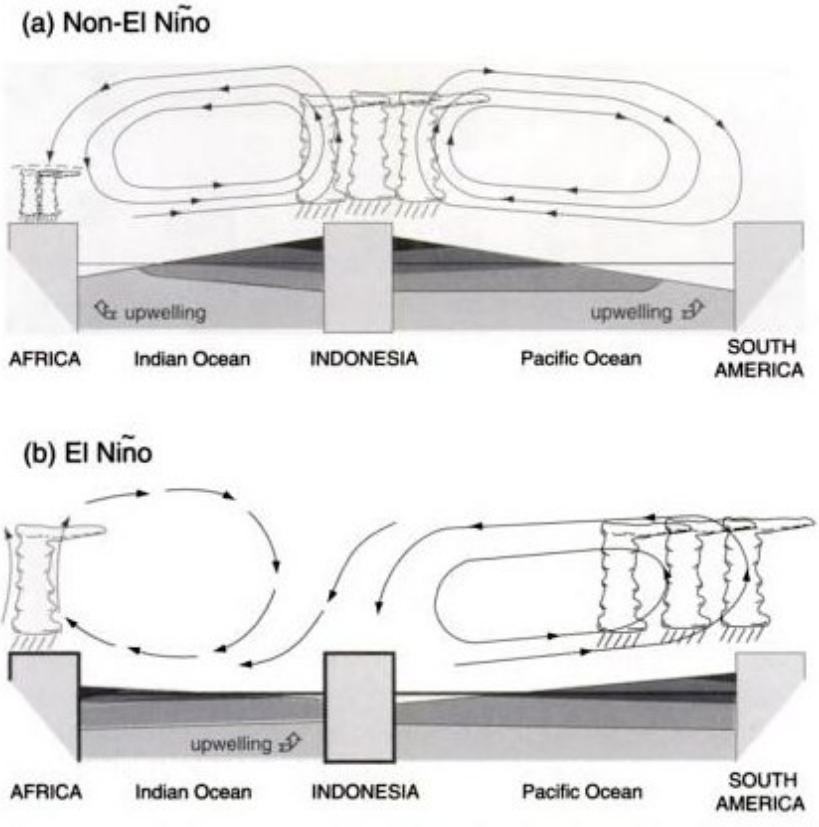
(a) Non-El Niño
upwelling
upwelling
AFRICA
Indian Ocean
INDONESIA
Pacific Ocean
SOUTH AMERICA
(b) El Niño
upwelling
AFRICA
Indian Ocean
INDONESIA
Pacific Ocean
SOUTH AMERICA

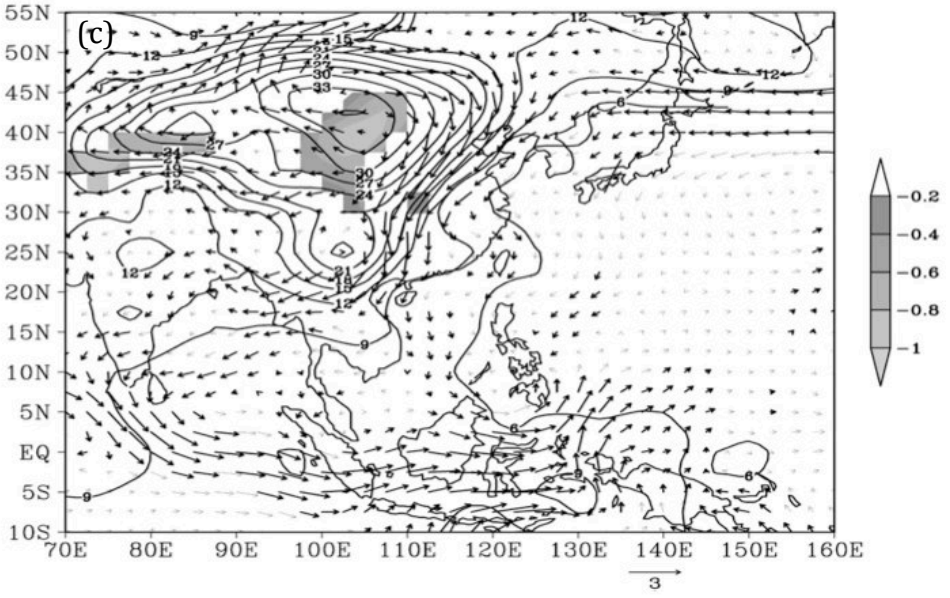
(c)
55N
50N
45N
40N
35N
30N
25N
20N
15N
10N
5N
EQ
5S
10S
70E
80E
90E
100E
110E
120E
130E
140E
150E
160E
3
−0.2
−0.4
−0.6
−0.8
−1

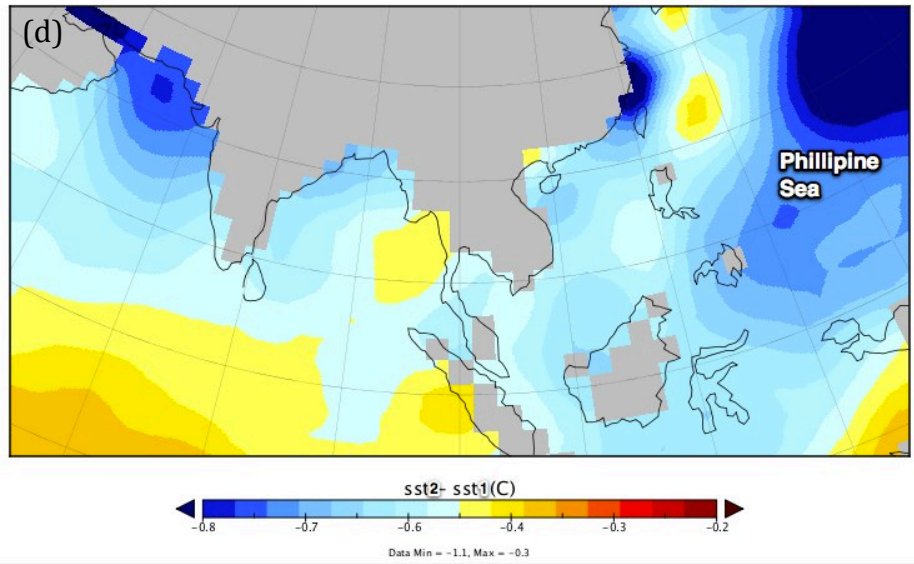

Fig. 7a, b: Schematic view of the change in wind fields along the equator across the Pacific and Indian Oceans during non- El Niño period and El Niño period; (Wang, 2006) c. Mean JJA wind vector (m/s) anomalies during ENSO events compared to non-El Niño years; dark vectors denote that the difference exceeds the 95% confidence level), and temperature (shaded; °C) fields at 850 hPa (Wang, 2006) d. Long term mean values of SST after1978 minus long term means before1978)

During non-El Niño years (Fig 7a), mean convection occurs over the warm pool in the western Pacific (around Phillipine Sea) and Indonesia. With El Niño (Fig. 7b), the weakened Walker cell leads to decreased convection, or even the change of the sign of vertical motions to subsidence over Indonesia. Wang et al. (2000) pointed out that the circulation system that conveys the impact of El Nino to East Asia is the anomalous Philippine Sea anticyclone (PSAC). Moreover, near surface wind anomalies over the NEASM region are northerly during El Niño events (Fig. 7c), which causes reduced water vapor and precipitation.

The changes associated with ENSO have several parallels in the decadal-scale changes associated with precipitation shifts around 1978. Not only was the SST in the Phillipine Sea colder (Fig. 7d), but there is also enhancement of a lower-level anticyclone in the same area after 1978 (Fig. 6c), similar to El Niño conditions. Subsidence increased over Indonesia after 1978 (Fig. 4b), and there was enhanced southward flow over the NEASM (Fig. 5f).

Via the Circum-Global Teleconnection (CGT), ENSO is connected with ISM, which is then connected with precipitation anomalies in the Mediterranean regions (Ding and Wang, 2004). In the next section, similar teleconnections at the decadal scale are considered.

5 Large-scale teleconnection mechanisms

The strength of the East Asian summer monsoon is closely correlated with intensities of the convective heat sources centered over Philippine Sea (Li et al., 2010). Chang also pointed out (2004) that abnormal water vapor transport flux over East Asia and tropical western Pacific around 1970s was caused by the "interdecadal variation of SST in the tropical Pacific". The SST anomalies will affect low-level atmospheric temperatures and sea level pressure gradients and in turn, the precipitation of the East Asia Monsoon regions by teleconnections.

The heating of NWP seawater contributes to the formation and maintenance of the upper tropospheric easterly jet, which then influences the strength of ISM. According to Rodwell and Hoskins (1996), diabatic heating in south Asia will cause the subsidence in

the Mediterranean region through a Rossby-wave pattern. Through this pattern the remote diabatic heating in the ISM region can induce adiabatic descent over eastern Sahara/Mediterranean and southeast of the Aral Sea. Descent is caused by the distorted isentropes and enhanced by the positive feedback with radiative cooling. With the easterly jet weakened after 1978 (Fig. 5b), weaker descent in those regions occurs as expected (Fig. 4a).

Enomoto et al. (2003) proposed a 'silk-road' pattern, which sets the teleconnection between Sahara/Mediterranean area and Japan. Potential Vorticity (PV) near the tropopause is transmitted to the east by Asian Jet, the northern fringe of the Tibetan anticyclone that develops during the Asian Monsoon, because PV is conservative. An equivalent-barotropic ridge (Bonin High) is formed at the exit of the Asian Jet at upper levels. Enomoto proposed this "Monsoon-Desert-Jet" system as the cause of Bonin High. The strength of this ridge near Japan is regulated by the intensity of Asian Jet. As the upper-level westerly flow gets weaker (Fig. 5a) and the "+-+-" pattern gets less pronounced (Fig. 5d), the upper level pressure near Japan and the NEASM are both decreased (Fig. 7a). This corresponds to the findings of Ding and Wang (2005) that without the presence of El Niño or La Niña, the correlation between CGT in mid-latitude of the North Hemisphere and ISM remains significant; with the abnormal SST, however, the relationship is weakened.

The SEASM is more directly affected by the SST anomaly in the Philippine Sea. Chang et al. (2000b) partitioned the NCEP reanalysis data set of 1951-1996 into two

periods, 1951-1977 and 1978-1996. They pointed out that the NWP subtropical ridge is stronger in the second period than the first, and is the main reason for the precipitation anomalies in the second period, especially in SEASM. The NWP subtropical ridge is caused by a positive feedback that involves the anomalous Hadley and Walker circulations. This anticyclone blocks the Mei-yu fronts from moving southward, thereby producing more stationary rainfall in the SEASM region. Additionally it enhances the pressure gradient to its north and northwest, resulting in a more intense front.

Also due to the persistence of the anticyclone, the western Pacific Subtropical Ridge extends farther to the west from the previous winter to the following summer, resulting in an anomalous anticyclone near the southeast coast of China, bringing abundant precipitation to SEASM region. This is testified by the abnormal northward wind on the South China Sea in Fig. 5f. This mechanism has been pointed out to be one of the main causes for the floods that occurred in the lower Yangtze River region after a peak El Niño (Ye and Huang 1996), another illustration of the parallels between conditions during post-1978 decades and the much shorter-term anomalies associated with El Niño events.

The above mechanism can be summarized in the flow chart in Fig. 8.

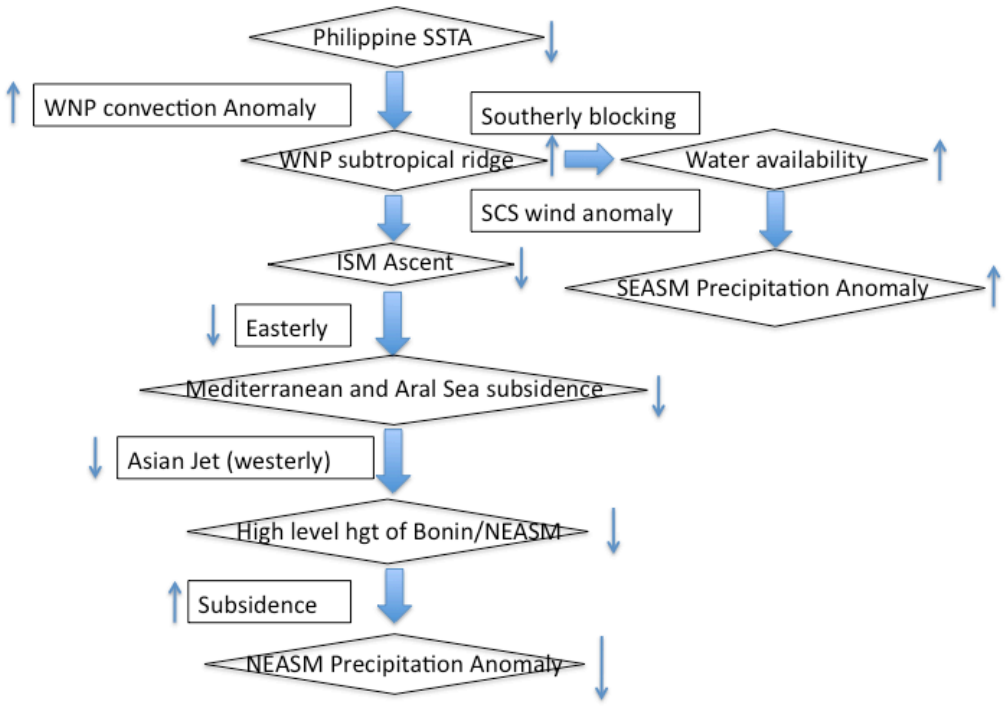

Fig. 8 Flow chart of the large-scale circulation contributing to EAM dipole

6 Precipitation anomalies of the last 1000 years

The conceptual model shown in Figure 8 was developed as a potential modern analogue for past out-of-phase changes in the core region of the East Asian monsoon and dry regions to the north that have been proposed on the basis of paleoclimatic research (e.g. Mason et al., 2009) Zhang et al. (1997) analyzed the wet and dry series over the past 1000 years in East China, pointing out that in general the lower reaches of Yangtze River is out of phase with the northern regions. In this section, the applicability of this modern analogue is evaluated using the past 1000 years. During that time period, basic circulation patterns and ocean-atmosphere relationships were not too different from the present.

General contrasts between the Medieval Warm Period (MWP) and Little Ice Age (LIA) are considered first. Recent studies have detected notable changes in the Asian monsoons during the transition from MWP to LIA, at centennial scales (e.g. Gupta et al, 2003). In East Asia, there is a variety of evidence that changes in precipitation at this time were in different directions in the NEASM and SEASM. Reconstruction of east China dry/wet conditions over the last 1000 years, using historical records, revealed that abrupt change occurred between the MWP and LIA, with the NEASM region changing from wet to dry (Zhang et al., 1997). In contrast, reconstruction of rainfall in the middle and lower reaches of the Yangtze catchment and in the South China, suggests increased precipitation during the LIA (Wang and Dong, 2002). A 2000 year fossil pollen series from Northeast China (NEASM) indicates a generally high level of summer rainfall during MWP (Ren, 1998), supporting the reconstruction by Zhang et al. (1997). In contrast geochemistry of dated sediment cores from Lake Huguangyan (21°N, 110°E) in SEASM region suggests that tropical South China was dry during the MWP and wet during the LIA (Chu et al., 2002).

The MWP was used as an example (Fig. 9 a and b) to compare precipitation indices of the EASM regions generated from cave records with near-annual resolution. The precipitation index of NEASM and SEASM regions generated from Wanxiang cave (33º19'N, 105º00'E, 1200 m above sea level) (Zhang et al., 2008) and Dongge cave (25°17'N, 108°5E, elevation 680 m) (Wang et al., 2008). They provide an estimate of the moisture index of the recent 1000 years. Using the same regime-shift analysis parameters that were applied to the NCEP data did not capture shifts that seemed

evident in the data, such as a shift around the year 1071 AD in the NEASM region. Thus, the cut-off length was modified to 20 years and the Huber's weight to 1 sigma. It is reasonable to modify the parameters in this case considering the longer period of time.

Comparison between Figure 9a and b reveal a partial out-of-phase pattern in regime shifts at pentadecadal (40–60 year) timescales. For example, the precipitation in the NEASM region shifts to a higher mean beginning at 1071 AD and lasting about 40 years, while SEASM shifts to lower precipitation beginning at about 1087 and lasting about 60 years. However, the out-of-phase pattern is not consistent across the time period shown and there are fairly large lags between shifts.

Based on correlation analysis, Wu and Wang (2002) pointed out that EASM decadal variation is concurrent with major shifts in tropical Pacific SST. This is proved to be significant in the oscillation mode for NEASM and SEASM during the past 1000 years, significant at the 95% confidence level (Shen et al., 2008). The time series of ENSO index (21-year running average) based on the work of Li et al. (2011) revealed also the 30 to 50 year oscillation during MWP (Fig 9c). Li et al. derived the ENSO index from the first principal component of tree-ring based North America Drought Atlas. Note that the ENSO oscillations don't match very well with the detected shifts of the precipitation index in Fig. 9 a and b, although they would be expected to be a factor in those switches according to the model in Fig. 8 and previous research (Wu and Wang, 2002).

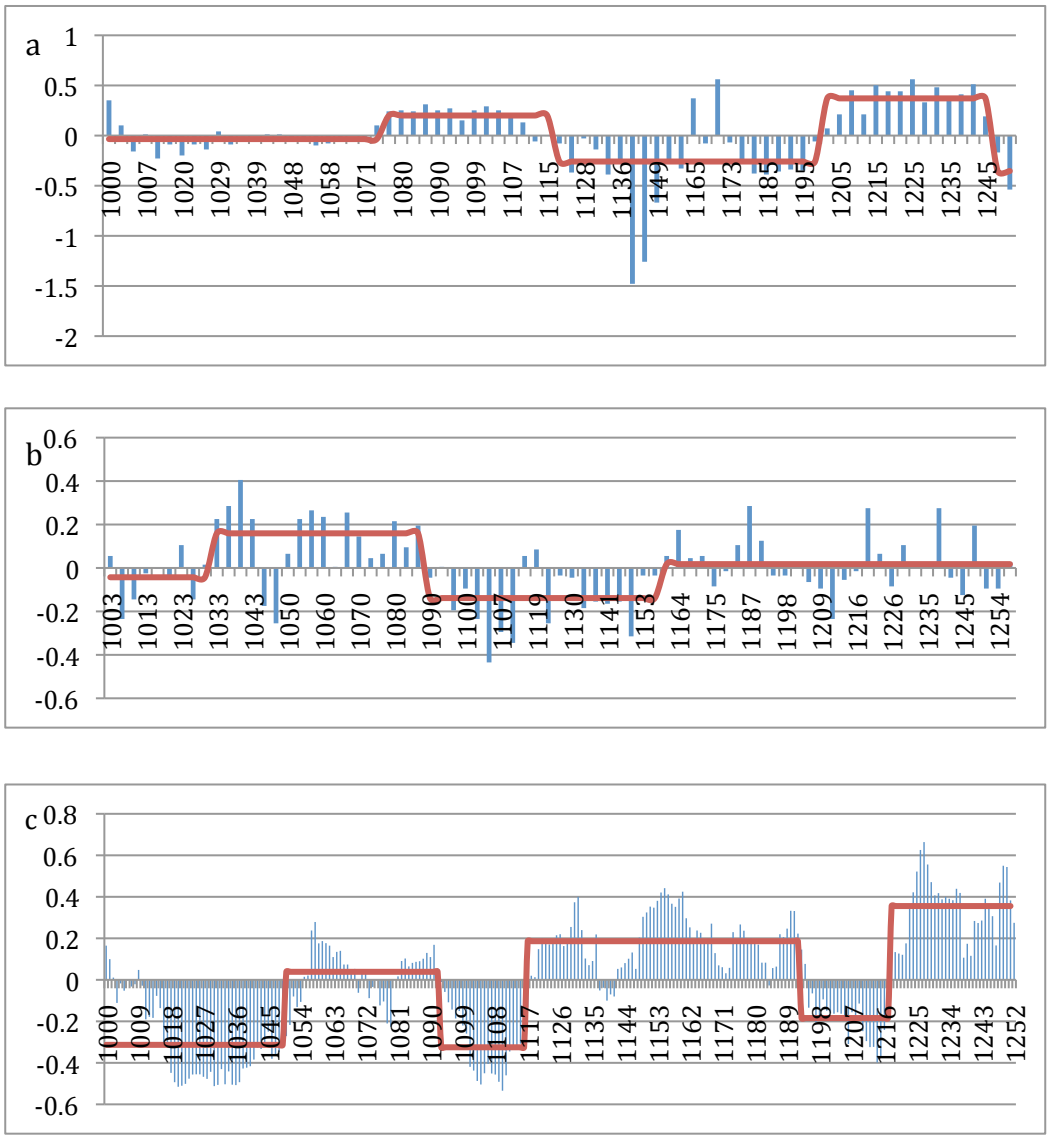

Fig. 9 Time series of precipitation index of a. SEASM b. NEASM and c. ENSO index during MWP. Red line: weighed values given by regime shift. Data sources: Zhang et al., 2008; Wang et al., 2005

Discussion and Questions for Further Research

The conceptual model shown in Figure 8 can potentially explain the overall contrast between the climates of the MWP and LIA in northern and southern East Asia monsoon regions. Proxy records indicate the MWP was relatively wet in the NEASM, while conditions were dry at the same time in the SEASM. Therefore, circulation patterns between 1948 and 1978 may provide a good modern analog for the MWP. Similarly, the period after 1978 may be a good analog for the LIA (dry in the north and west in the south). On the other hand, high-resolution proxy records do not clearly show the same out-of-phase pattern, nor the expected relationship with ENSO, at decadal timescales within the MWP. It is possible that other mechanisms influence decadal-scale precipitation shifts during the MWP, as opposed to larger changes between the MWP and LIA. The high-resolution reconstructions that were used may also be inaccurate, which can only be judged when more proxy records with the same resolution have been developed.

This research raises several questions that could be the subject of future work:

1. Role of the PDO

The interdecadal variation of the Pacific Decadal Oscillation (PDO) modulates the East Asian monsoon via its impact on the El Niño-Southern Oscillation (ENSO) (Wang et al., 2008). Several studies have characterized the PDO as emerging from a phase-locked interaction between oscillations with 20 and 50 year periods, and regime shifts occur

when the oscillations change phase simultaneously (Nakamura et al., 1997; Minobe, 1999, 2000). Wang (2006) points out that the Pacific Oscillation exerts influence to EAM by SST anomalies of Philippine Sea. With the PDO index shifting also around the year 1976 (Fig. 10a), it's possible that PDO has a role in decadal shifts of the precipitation dipole in the EAM region. According to Wang and Zhang (2002), the developing El Niño induces off-equatorial ascending Rossby wave responses and land surface cooling in northeast Asia; both deepening the east Asian trough in fall and inducing vigorous tropical–extratropical exchange of air mass and heat, which enhances the cold air outbreak and initiation of the Philippine Sea anticyclone.

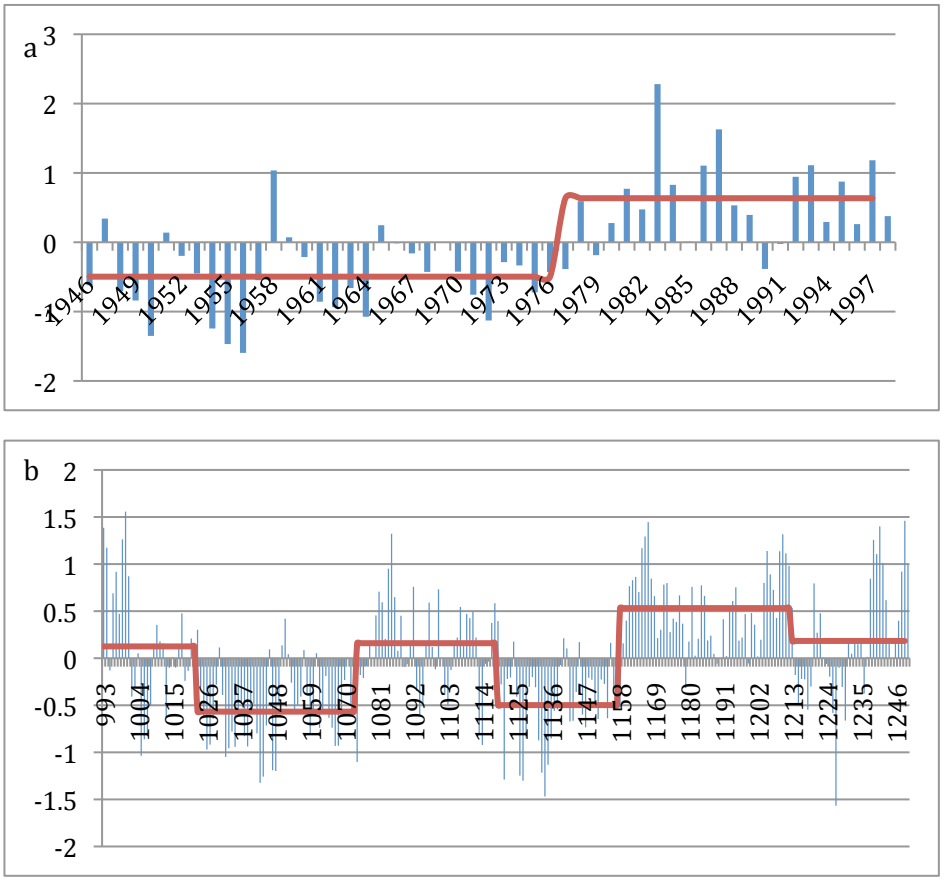

Fig. 10 PDO index of a. recent 48 years and b. MWP (data source: Jungclaus et al., 2010). Red line: weighed values given by regime shift.

2. Lag between the shifts of NEASM and SEASM

The out-of-phase pattern between NEASM and SEASM is apparent in Fig. 3a and b, but a lag of about 8 years exists between regime shifts in the two regions. Shifts in the high-resolution precipitation reconstructions for the MWP have longer lags; in fact, the timing between shifts is different enough that an alternative interpretation is possible: the abrupt shift to dry conditions of SEASM region happens around 1125AD, which can be viewed as a lag from the shift to dry around 1090AD for NEASM. Then this dry episode lasted for approximately 60 years for both NEASM and SEASM. Clearly, more information is needed on the validity and representativeness of MWP reconstructions before this issue can be resolved.

3. Long-term phase relations between northern and southern East Asian Monsoon regions.

A 284,000-year long transient simulation for precipitation using FOAM GCM models shows an in-phase pattern between SEASM and the Indian Summer Monsoon, yet an out-of-phase pattern between NEASM and ISM. More specifically when it's wet for south China monsoon area, its northern neighboring area is dry with the orbital forcing of obliquity (Chen et al., 2010). The obliquity anomaly triggers the ISM anomaly and a series of teleconnections following it, and the out-of-phase pattern between

NEASM and SEASM is then established. More work is needed on the connection between these long-term relations and the decadal out-of-phase shifts identified by modern analog analysis.

Conclusion

By analyzing the NCEP reanalysis data for the past 63 years (1948-2010), the present research identifies a shift in moisture index from wet to dry for NEASM around 1977, with the opposite shift for SEASM around the year 1986. Both local subsidence/uplift patterns and larger scale circulations contribute to this dipole system. The index for vertical motion (omega) in the EAM region reveals the abnormal ascent in the south and descent in the north after the year 1977. Thus the convection is enhanced in SEASM and decreased in NEASM. Anomalies in zonal index (uwind/vwind), pressure index (geo-potential height), vertical index (omega) and ENSO index (SST) implies a larger scale atmospheric circulation system that also contributes to the dipole.

The ocean surface cooling around 1978 near the Philippine Sea, which correlates with ENSO events, is the triggering factor of the whole process. The convection anomaly that results in the western Pacific suppresses Indian Summer Monsoon and associated ascent in the ISM region. This anomaly is transported to the west through the teleconnection between ISM and the Mediterranean/Aral Sea region; this in turn results in a decreased Asian Jet, and less effective transmission of PV from the west back to NEASM through “silk-road pattern”. The effect is less-than-normal precipitation in the NEASM region. The SEASM, on the other hand, is affected

mostly by the abnormal meridional wind originated from the SST anomaly in Philippine Sea. This anomaly also blocks the wind southward, which provides abnormally abundant water vapor.

This mechanism may also serves as an effective way for explaining the precipitation anomalies at hundred- to- thousand year scales. In particular, the contrasting climates of the Medieval Warm Period and Little Ice Age in northern and southern China appear to represent a similar dipole as found in modern observations.

Bibliography

1. Aguado, Edward, and James E. Burt. 2009. Understanding Weather and Climate. 5th ed. Prentice Hall.
2. Chang, C-P., Zhang Y.S., and Li T., 2000a. Interannual and Interdecadal Variations of the East Asian Summer Monsoon and Tropical Pacific SSTs. Part I: Roles of the Subtropical Ridge. Journal of Climate 13:4310-4325.
3. Chang, C-P., Zhang Y.S, and Li T., 2000b. Interannual and Interdecadal Variations of the East Asian Summer Monsoon and Tropical Pacific SSTs. Part II: Meridional Structure of the Monsoon. Journal of Climate 13: 4326-4340.
4. Chang C. P., 2004. East Asian Monsoon. World Scientific Press, ISBN: 981-238-769-2
5. Clemens, S. C., Wang, P., and Prell, W. L., 2003. Asian monsoons and global linkages on milankovitch and sub-milankovitch time scales, Mar. Geol., 201, 1–250, 2003.
6. Crowley, T.J., and T. Lowery, 2000. How Warm Was the Medieval Warm Period? Ambio, 29, 51-54.
7. Ding, Q. and Wang, B., 2005. Circum global Teleconnection in the Northern Hemisphere Summer, Journal of Climate 18 (17): 3483-3505.
8. Enomoto. T, Hoskins. B.J., and Matsuda. Y, 2003. The formation mechanism of the Bonin high in August, Q. J. R. Meteorol. Soc., 129, pp. 157–178
9. Goswami, B. N. 2006. The Asian monsoon: interdecadal variability, in: The Asian Monsoon, edited by: Wang, B., Springer-Verlag, Berlin, 295–326
10. Gupta, A.K., Anderson, D.M., Overpeck, J.T., 2003. Abrupt changes in the Asian southwest monsoon during the Holocene and their links to the North Atlantic Ocean. Nature 421, 354–357.

11. Gupta, A.K., Das, M., and Anderson, D.M., 2005. Solar influence on the Indian summer monsoon during the Holocene, Geophys. Res. Lett., 32, L17703
12. Harrison, S. P., Kutzbach, J. E., Liu, Z., Bartlein, P. J., Muhs, D., Prentice, I. C. & Thompson, R. S. (2003) Mid-Holocene climates of the Americas: a dynamical response to changed seasonality. Climate Dynamics, 20, 663-688.
13. Higgins RW, Mo K C, Yao Y, 1998. Interannual variability of the US summer precipitation regime with emphasis on the southwestern monsoon. J Clim 11: 2582–2606
14. Higgins RW, Shi W, 2000. Dominant factors responsible for interannual variability of the summer monsoon in the southwestern United States. J Clim 13: 759–776
15. Hodell D. A., Brenner M., Curtis J. H., Guilderson T., 2001, Solar Forcing of Drought Frequency in the Maya Lowlands David, Science 292, 1367
16. Hu, C., G.M. Henderson, J. Huang, S. Xie, Y. Sun, and K.R. Johnson. 2008. Quantification of Holocene Asian monsoon rainfall from spatially separated cave records. Earth and Planetary Science Letters, Vol. 266, pp. 221-232, Issues 3-4, 29
17. Huang R, Zhang R, Zhang Q. 2000. The 1997/98 ENSO cycle and its impact on summer climate anomalies in East Asia. Advances in Atmospheric Sciences 17: 348–362
18. Huang, R. H., 2001. Decadal variability of the summer monsoon rainfall in East Asia and its association with the SST anomalies in the tropical Pacific. CLIVER Exchange,2, 7-8
19. Huang, R.H. and Sun, F.Y. 1992. Impact of the tropical western Pacific on the east Asian summer monsoon. Journal of Meteorological Society of Japan 70, 243–56.

20. Jungclaus, J.H., S.J. Lorenz, C. Timmreck, et al., 2010. Climate and carbon-cycle variability over the last millennium. Clim. Past, 6, 723-737. doi:10.5194/cp-6-723-2010
21. Kistler, R., Kalnay, E., Collins, W., Saha, S., White, G., Woollen, J., Chelliah, M., Ebisuzaki, W., Kanamitsu, M., Kousky, V., van den Dool, H., Jenne, R., Fiorino, M., 2001. The NCEP-NCAR 50-year reanalysis: monthly means CD-ROM and documentation. Bulletin of the American Meteorological Society 82, 247–267.
22. Kumar, K., Rajagopalan, B., Hoerling, M., Bates, G., Cane, M., 2006. Unraveling the mystery of Indian monsoon failure during El Niño. Science 314, 115–119.
23. Lamb, H.H. 1977. Climate: present, past and future. Vol. 2: climatic history and the future. London: Methuen.
24. Lau, K. –M., and H.-Y. Weng, 2001. Coherent modes of global SST and summer rainfall over China: An assessment of the regional im- pacts of the 1997/98 El Niño. J. Climate, 14, 1294–1208
25. Li, J., S.-P. Xie, E.R. Cook, G. Huang, R. D'Arrigo, F. Liu, J. Ma, and X.-T. Zheng. 2011. Interdecadal modulation of El Niño amplitude during the past millennium. Nature Climate Change, Vol. 1, Issue 2, pp. 114-118, May 2011, doi:10.1038/nclimate1086
26. MacDonald G., 2011, Potential influence of the Pacific Ocean on the Indian summer monsoon and Harappan decline. Quaternary International, 229, 140–148
27. Mason, J.A., H. Lu, Y. Zhou, X. Miao, J.B. Swinehart, Z. Liu, R.J. Goble, and S. Yi. 2009. Dune mobility and aridity at the desert margin of northern China at a time of peak monsoon strength. Geology 37 (10) : 947-950
28. Minobe, S., 2000.Spatio-temporal structure of the pentadecadal variability over the North Pacific, Prog. Oceanogr., 47, 381–408

29. Mock, C.J., Bartlein, P.J., 1995. Spatial variability of late-Quaternary paleoclimates in the western United States. Quaternary Research 44, 425–433.
30. Mock, C.J., Brunelle-Daines, A.R., 1999. A modern analogue of western United States summer paleoclimate at 6000 years before present. Holocene 9, 541–545.
31. Nitta, T., and S. Yamada, 1989. Recent warming of tropical sea surface temperature and atmospheric flow patterns. J. Meteor. Soc. Japan, 67, 375-383
32. Ren G, 1998. Pollen evidence for increased summer rainfall in the Medieval warm period at Maili, Northeast China. Geophysical Research Letter. Vol. 25, No. 11. 1931-1934
33. Rodionov, S.N., 2006. The use of prewhitening in climate regime shift detection, Geophys. Res. Lett., 31, L12707, doi:101029/2006GL025904.
34. Shen C., Wang W.C., Peng Y. et al., 2008. Variability of summer precipitation over eastern China during the last millennium, Clim. Past Discuss., 4, 611–643
35. Shinker, J.J., Bartlein, P.J. & Shuman, B., 2006. Synoptic and dynamic climate controls of North American mid-continental aridity. Quaternary Science Reviews, 25(13-14), 1401-1417.
36. Shukla, J. 1998. Predictability in the midst of chaos: a scientific basis for climate forecasting. Science 282, 728–31.
37. Tan, L., Y. Cai, L. Yi, Z. An, and L. Ai. 2007. Precipitation variations of Longxi, northeast margin of Tibetan plateau since AD 960 and its relationship with solar activity. Climate of the Past Discussions 3, no. 5: 1037–1061.
38. Trenberth, K.E. and Hurrell J.W., 1994. Decadal atmosphere-ocean variations in the Pacific. Climate Dyn., 9,303-319

39. Waliser, D. E., 2006.Intraseasonal variability, in: The Asian Monsoon, edited by: Wang, B., Springer- Verlag, Berlin, 203–257.
40. Wang B., Wu R., Lukas R. et al., 2001: A possible mechanism for ENSO turnabout. Dynamics of Atmospheric General circulation and Climate, IAP/Academia Sinica, Ed., China Meteorological Press, 552–578
41. Wang L., Chen W., and Huang R., 2008, Interdecadal modulation of PDO on the impact of ENSO on the east Asian winter monsoon, Geophysical Research Letters, Vol. 35, L20702doi: 10.1029/2008GL035287
42. Wang, B., 2006. The Asian Monsoon, Springer/Praxis Publishing Co., New York
43. Wang. B, Wu R., and Fu X., 2000. Pacific–East Asian teleconnection: How does ENSO affect East Asian climate? J. Climate, 13, 1517–1536.
44. Wang, B. and Lin, H., 2002: Rainy seasons of the Asian-Pacific monsoon. J. Climate, 15, 386-398
45. Wang, Y., H. Cheng, R.L. Edwards, Y. He, X. Kong, Z. An, J. Wu, M.J. Kelly, C.A. Dykoski, and X. Li. 2005. The Holocene Asian Monsoon: Links to Solar Changes and North Atlantic Climate. Science, Vol. 308, pp. 854, 6 May 2005.
46. Wright, R.P., Bryson, R.A., Schuldenrein, J., 2008. Water supply and history: Harappa and the Beas regional survey. Antiquity 82, 37–48.
47. Yang, S., and Lau, K.-M., 2006. Interannual variability of the Asian monsoon, in: the Asian monsoon, edited by: Wang, B., Springer-Verlag, Berlin, 259–293
48. Yao T., Thompson, L.g., Qin D., Tian L., Jiao K., Yang Z., Xie C., 1996. Variations in temperature and precipitation in the past 2000a on the Xizang (Tibet) Plateau – Guliya ice core record, Vol. 39 No. 4, 425-433

49. Ye, D. Z., and R. H. Huang, 1996. Study on the regularity and formation reason of drought and flood in the Yangtze and Huaihe River regions (in Chinese). Shandong Sci. and Tech. Press, 387 pp.
50. Zahn, R., 2003. Monsoon linkages. Nature 421, 324–325
51. Zhang, D.E., Liu, C.Z., Jiang, J.M., 1997. Reconstruction of six regional dry/wet series and their abrupt changes during the last 1000 years in East China. Quaternary Sciences, 1–11 (in Chinese with English Abstract).
52. Zhang, P. et al., 2008. A test of climate, sun, and culture relationships from an 1810-year Chinese cave record. Science 322, 940–942
53. Zhu, W. and Wang, S., 2002. 80yr oscillation of summer rainfall over North China and East Asia summer monsoon, Geophys. Res. Lett., 29, 1672, doi:10.1029/2001GL013997

Appendix

```
# The code for generating the long-term mean file using the data
for each year from 1948 to 2010 – using 500mb level Uwind as an
example.

# Define dimensions
a=c(seq(0,180,by=2.5),seq(-177.5,-2.5,by=2.5))
b=c(seq(90,-90, by=-2.5))
d=c(10,20,30,50,70,100,150,200,250,300,400,500,600,700,850,925,1000
)
x <- dim.def.ncdf( "Lon", "degreesE",a)
y <- dim.def.ncdf( "Lat", "degreesN",b)
t <- dim.def.ncdf( "Time", "year", 1, unlim=TRUE)
l <- dim.def.ncdf( "level", "mb", 6)

# Make a variable with those dimensions.
ltmuwind <- var.def.ncdf("uwnd", "m/s", list(x,y,l,t), 1.e30)

#create a netCDF fie
ncnew<-create.ncdf("500uwnd1.ltm.nc",ltmuwind)

#obtain data from file
monuwnd=open.ncdf("uwnd.mon.mean.nc")
ltmo=array(data=0,c(144,73,1,1),c("long","lat","level","time"))
for (i in seq(1,144)) {
    for (j in seq(1,73)) {
     for (k in 1:63){
          for (t in 5:7)
     {p=t+k
          ltmo[i,j,1,1]=ltmo[i,j,1,1]+ get.var.ncdf(monuwnd, varid
= "uwnd", start = c(i,j,6,p), count = c(1,1,1,1))
     }
     }
     ltmo[i,j,1,1]=ltmo[i,j,1,1]/3/63

}
}
#write data to the new file
put.var.ncdf(ncnew,ltmuwind,ltmo)


#Code for generating the time series for NEASM and SEASM regions –
using the precipitation rate (prate) of NEASM as an example.
```

```
#read the data:
mprecip <- open.ncdf("prate.mon.mean.nc")
ltmprate=open.ncdf("prate.mon.ltm.nc")

#set the regions:
for (i in seq(110.625,118.025,1.875)) {
    for (j in seq(35.237,40.952,1.904)){
     yrprecip <- matrix(1:65, ncol=65)
# inner loop over 63 years:
     for (k in 1:63) {
          time <- (k*12)-6
          yrprecip[k+2] <- (get.var.ncdf(mprecip, varid = "prate",
start = c(i,j,time), count = c(1,1,1))-
get.var.ncdf(ltmprate,varid="prate",start=c(i,j,6),count=c(1,1,1))+
get.var.ncdf(mprecip, varid = "prate", start = c(i,j,time+1), count
= c(1,1,1))-
get.var.ncdf(ltmprate,varid="prate",start=c(i,j,7),count=c(1,1,1))+
get.var.ncdf(mprecip, varid = "prate", start = c(i,j,time+2), count
= c(1,1,1))-
get.var.ncdf(ltmprate,varid="prate",start=c(i,j,8),count=c(1,1,1)))
/3
     }
     yrprecip[1] <- i
     yrprecip[2] <- j
     write(yrprecip, file="NEASM.csv", sep=",", ncolumns=65,
append=TRUE)
    }
}
```